Simulation of Biodiesel Jet in Cross Flow

E. Farvardin, A. Dolatabadi[1*]
Mechanical Engineering Department, Concordia University, Canada
e_farva@encs.concordia.ca and dolat@encs.concordia.ca

Abstract

Near field behaviour of a liquid jet in crossflow, i.e. deformation, primary breakup and penetration is investigated. Biodiesel, diesel and their blend are used as the liquid jets entering the crossflow of air. In this study, the primary breakup of biodiesel jet is simulated using the Volume of Fluid (VOF) numerical method. In order to, accurately, capture vortices including the horseshoe vortex in the gas and the liquid internal vortices, Large Eddy Simulation (LES) turbulence model is coupled with the VOF. The operating condition of this study is gas Weber number of 48 and 80 with a liquid to gas momentum ratio of 50 and 100. This work serves as a comparative study of biodiesel and diesel spray characteristics in crossflow. The results show lower penetration depth of biodiesel comparing to diesel that agree well with the previous experimental work of the authors [1].

Introduction

Liquid jet in cross flow has many applications such as in gas turbine combustion chamber, ramjets, scramjets and agriculture industry. Furthermore, it can be served as a fundamental study of spray quality for different fuels as it illustrates jet disintegration, surface waves, primary and secondary breakups, effect of viscosity, effect of surface tension and the effect of density of the fuel on the final droplet size distribution, mixing, evaporation and combustion processes. In the last decade, scientists and industries have been attracted to the use of renewable energy such as biofuels. Biodiesel as an alternative for diesel, which is already in use by many industries such as transportation and energy, played a pioneer role in this direction. Moreover biodiesel has different renewable resources including Canola oil, cottonseed oil, animal fat, soybean oil, yellow grease and brown grease. Contrary to these advantages, the ignition, atomization and evaporation of biodiesel have been critiqued [2-3]. In a recent comparative study by the authors [1], it has been shown experimentally that biodiesel has lower penetration depth comparing to diesel. The lower penetration depth is thought to be as a reason of primary breakup and jet column bending before the disintegration [1]. In this numerical study, deformation, surface waves, and disintegration of a set of biodiesel blend jets issued from the same orifice are compared with those of a diesel jet.

One of the first works on Liquid Jet in Cross Flow (LJICF) is the experimental studies of Schetz and Padhye [5]. They conducted a series of experimental tests in order to find the locus of column jet breakup at different momentum ratios. Finally they proposed a correlation for the jet column breakup versus the momentum ratio, drag coefficient and the fluids length scales. Thereafter, one of the most cited works in the area is performed by Wu *et al.* [6-8]. They proposed a new breakup map for liquid jets in crossflow based on the Weber number of the gas. In addition, a series of tests were conducted by them on water, glycerol and ethanol in order to take account the effects of viscosity and surface tension. Furthermore, they correlated the windward trajectory of spray and breakup length to the momentum ratio; however the correlation does not contain viscosity and Weber number. Following these works, Stenzler *et al*. [10] found that viscosity and Weber number can directly affect the trajectory and penetration of sprays in crossflow and they included these effects into their proposed correlation. They tested water, kerosene, acetone and 4-heptanone. In this vein, Farvardin *et al.* [1] modified the correlation of Stenzler *et al.*, by considering the high viscosity associated with biodiesel and its blends. They conducted a series of shadowgraph and PDPA experiments in order to find and compare the trajectories of traverse liquid jets in a subsonic crossflow of air. Diesel, biodiesel, and their blends were injected at different gas Weber numbers (from 11 to 80) and liquid-to-gas momentum ratios (from 10 to 135). Ultimately, they found a remarkable change in the trajectory of biodiesel jet in crossflow comparing to that of diesel. However, they found that the droplet size distributions do not differ significantly. Accordingly, they concluded that the difference in the trajectories can be a result of the primary breakup and deflection of the jet column before the primary and secondary breakups [1].

* Corresponding author: dolat@encs.concordia.ca

From the numerical point of view, Madabhushi [11] performed a series of Lagrangian particle tracking simulations of droplets in a gaseous crossflow. He used a Reynolds Average Navier-Stokes coupled with k-ε turbulence model for the gaseous part and validated his results with an experimental work. Although a general agreement with the experiment was observed, due to the absence of wakes and vortices which are mostly damped by k-ε model, some of the droplets' velocity and size were different from the experiment. Subsequently Aalborg *et al*. [12] performed a Volume of Fluid numerical modelling of LJICF. A correlation between the wavelength, jet diameter and Weber number was obtained based on their study. Later on, Hermann [13] developed a Refined Level Set Grid (RLSG) method, which is coupled with Large Eddy Simulation (LES) turbulence model, for capturing the liquid interface of the jet in crossflow. He also has added on a Lagrangian two way coupled simulation for small and spherical droplets downstream of the jet primary breakup.

In this study, the near field of the injection point is simulated numerically. The main aim of this work is to compare the primary breakup of biodiesel, diesel and their blend, in order to find out why biodiesel and its blends have different trajectories and subsequently penetration depth. In this regard, the same geometry of orifice and operating condition are used as [1]. The simulations are performed at Weber numbers 48 and 80 which represent the bag and multi-mode regimes of liquid breakup in gaseous crossflow. In addition the momentum ratio is kept at 50 and 100.

Geometry and Boundary Conditions

Figure 1 schematically shows the computation domain and boundary conditions. The liquid jet is injected from a plain circular orifice of 0.5 mm diameter. The flow inside the orifice is not modeled and just its exit is considered as a circular hole on top of the domain. In order to capture a wide domain around the near field of injection point, a domain of 10x40x40 times of the injector diameter is modeled in the lateral, horizontal and vertical directions respectively. As can be observed in Figure 1, the top wall is considered as a no-slip boundary condition (i.e. wall of the test section) and the remaining lateral sides can be inlet or outlet of air/water depending on the calculated pressure/velocity at those faces. The original mesh size at the initial time step is 0.1 mm hexahedral; however the dynamic mesh refinement, which is elaborated in the Methodology section, refines the mesh size in the locus of air/water interface at each iteration.

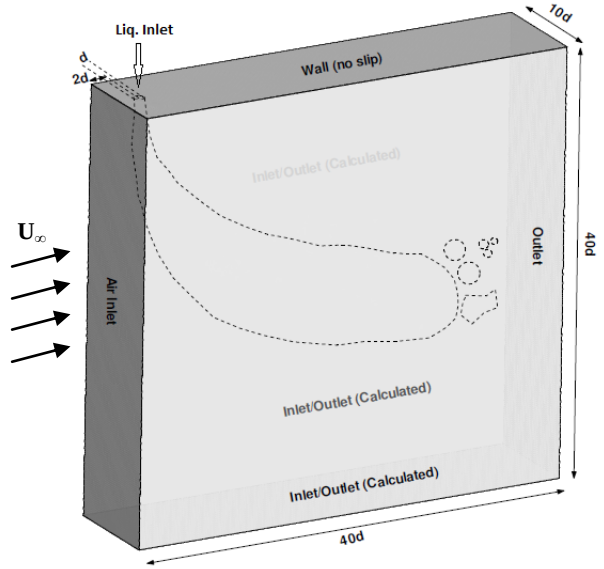

Figure 1 Schematics of the computational domain. (Not to scale)

Diesel, biodiesel (B100) and B50 blend are studied for several momentum ratios and Weber numbers. The blends are named based on the percentage of mass ratio of biodiesel to diesel. For example, B50 is made by 50% by mass of biodiesel added to 50% by mass of diesel. The physical properties of biodiesel (B100) are specified in Table 1 [14-15]. Additionally, the properties of B50 are interpolated between the properties of diesel and B100. As depicted in Table 1, the surface tension of B100 and B50 do not differ significantly from diesel; however the viscosity of B100 differs remarkably. In addition, the heat of combustion of B100 is almost 15% lower than the heat of combustion of diesel. Owing to this fact, in terms of comparison of two fuels, the mass flow rate of biodiesel should be higher than diesel in order to obtain the same heating value. This results into a biased operating condition as clarified in Table 2.

Table 1. Physical properties of diesel, biodiesel and blend

Properties	Diesel	B50	B100
Density (kg/m^3)	850	867	884
Surface Tension (N/m)	0.0252	0.02615	0.0271
Kinematic Viscosity (m^2/s)	1.40E-06	2.8E-06	4.20E-06
Heat of Combustion (BTU/lb)	19672	18151	16630

Table 2. Operating Condition

Parameters	Diesel	B50	B100
V_g (m/s)	45, 58	45, 58	45, 58
T_g (°C)	20	20	20
We_g	48, 80	48, 79	46, 76
q	50, 82	58, 94	67, 102

Methodology

In order to capture the primary breakup, secondary breakup, column jet disintegration and liquid jet surface waves, the numerical modeling is performed using the Volume of Fluid (VOF) method. In addition, Large Eddy Simulation (LES) turbulence model is utilized in order to accurately, capture the vortices upstream and down-stream the liquid jet, its drag and consequently the jet penetration. The governing equation for this modeling is the incompressible Navier Stokes equations including continuity and momentum equations with $\vec{v}$, ρ, p, μ and g as velocity, density, pressure, viscosity and gravity respectively.

$$\nabla.\vec{v} = 0 \tag{1}$$

$$\frac{\partial}{\partial t}(\rho\vec{v}) + \nabla.(\rho\vec{v}\vec{v}) = -\nabla p + \nabla.[\mu(\nabla\vec{v} + \nabla\vec{v}^T)] + \rho\vec{g} + \vec{F} \tag{2}$$

It should be mentioned that density and viscosity in each cell is calculated based on the volume fraction of that cell (α). Accordingly, the value of α is zero at the gas containing cells, one at liquid containing cells and between zero to one on the mixed containing cells [16]. Also $\vec{F}$ is the surface tension force on the interfacial cells which is a function of surface tension σ, surface curvature κ and the gradient of volume fraction α.

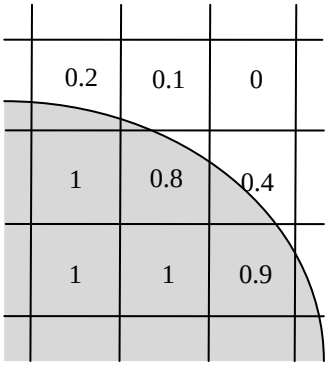

Figure 2 Schematic of VOF method on computational cells

$$\rho = \rho_l + \rho_g(1-\alpha) \tag{3}$$

$$\mu = \mu_l + \mu_g(1-\alpha) \tag{4}$$

$$\vec{F} = \sigma\kappa\nabla\alpha \tag{5}$$

$$\kappa = -\nabla.\left(\frac{\nabla\alpha}{|\nabla\alpha|}\right) \tag{6}$$

In order to account for the Large Eddy Simulation the Sub-Grid Scale (SGS) stress tensor comes from the nonlinear part of the convective term in the momentum equation. The SGS stress tensor can be approximated by means of the eddy viscosity definition and SGS kinematic viscosity. These two parameters in turn have a transport equation introduced by Yoshizawa and Horiuti [17].

$$\tau_{sgs} = \overline{\bar{v}\bar{v}} - \bar{v}\bar{v} \tag{7}$$

$$\tau_{sgs} - \frac{2}{3}k_{sgs}I = -\frac{\mu_{sgs}}{\rho}[\nabla\bar{v} + (\nabla\bar{v})^T] \tag{8}$$

$$\frac{\partial k_{sgs}}{\partial t} + \nabla.\left(k_{sgs}\bar{v}\right) = \nabla.\left[(\vartheta + \vartheta_{sgs})\nabla k_{sgs}\right] - \epsilon - \vartheta_{sgs}\bar{S}^2 \tag{9}$$

where in this equation ε, ν_{sgs} and S are found from the following relations.

$$\epsilon = \Delta C_\epsilon (k_{sgs})^{3/2}, \qquad C_\epsilon = 1.05 \tag{10}$$

$$\vartheta_{sgs} = \Delta C_k (k_{sgs})^{1/2}, \qquad C_k = 0.07 \tag{11}$$

$$\bar{S} = \frac{1}{2}(\nabla \bar{v} + (\nabla \bar{v})^T) \tag{12}$$

In terms of finding the interface of the two phases, in this study, a modified VOF method is used which has an additional convective term in the left hand side of the volume fraction conservation equation [18].

$$\frac{\partial}{\partial t}(\alpha) + \nabla.(\alpha \vec{v}) + \nabla.[\overrightarrow{v_r}\alpha(1-\alpha)] = 0 \tag{13}$$

The last term which is called artificial compression term contains the compression velocity which is computed in a suitable way to avoid smearing of the phase interface [19]. In this regard, since the multiplication with $\alpha(1-\alpha)$, this term has non zero value in the vicinity of the interface, it is calculated based on the Rusche's model [18].

$$\overrightarrow{v_{r,f}} = n_f min\left[C_\alpha \frac{|\varphi|}{|S_f|}, max\left(\frac{|\varphi|}{|S_f|}\right)\right] \tag{14}$$

Where φ, S_f, C_α and n_f are the face volume flux, cell face area vector, compression coefficient and face unit normal flux respectively. The face unit normal also is defined by the below equation.

$$n_f = \frac{(\nabla\alpha)_f}{\left|(\nabla\alpha)_f + \delta_n\right|} \tag{15}$$

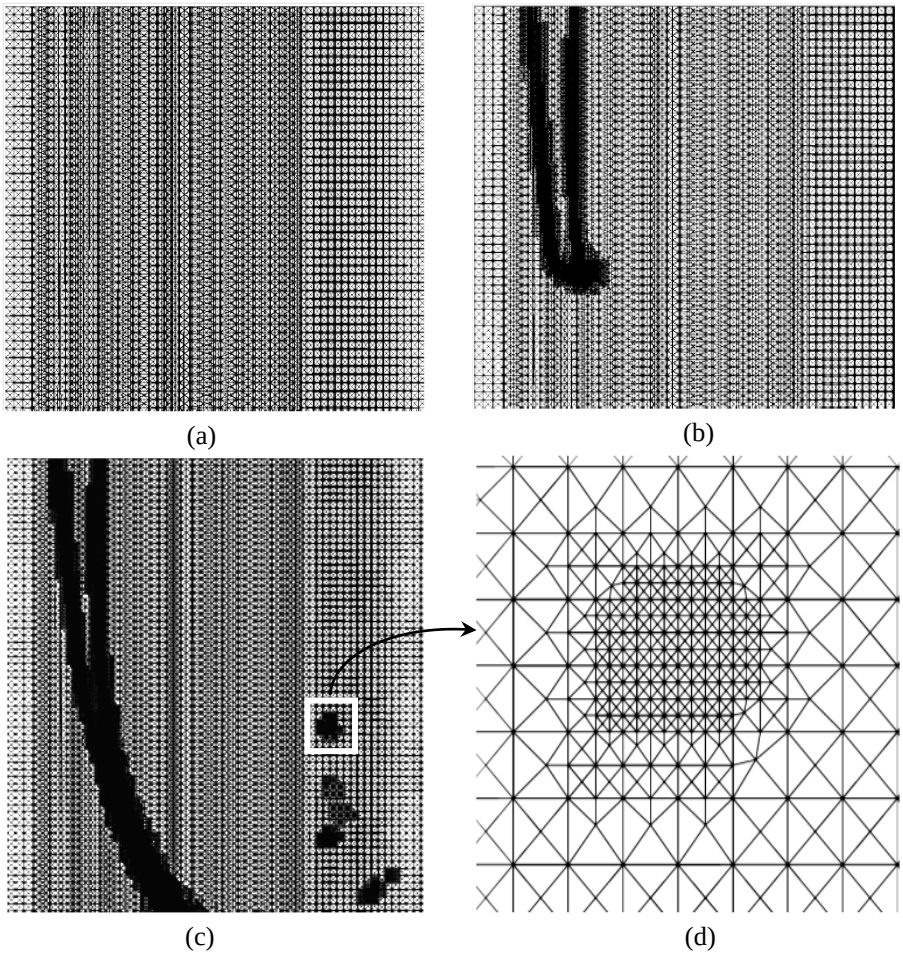

Figure 3 (a), Initial mesh cut-off, containing the injector exit, (b), dynamic refined mesh of cells with $0.01<\alpha<0.99$ (interface) at an intermediate time step, (c), dynamic refined mesh of cells with $0.01<\alpha<0.99$ (interface) after liquid jet advancement, (d), a close-up of mesh refinement

In addition, to solve the problem by means of the above formulation, for accurate tracking of the liquid interface, its surface waves, and breakup phenomenon, the interface has been captured by a dynamic adaptive mesh refinement method (OpenFoam CFD code [20]). The cells with volume fraction between 0.01 to 0.99 are refined while the rest of the mesh is retained at the original size (see Figure 3). In this manner, the liquid containing cells become finer at each iteration; however to have a reasonable computational time, a limit of maximum three refinement levels has been applied for each cell. Furthermore, a limiter of 10,000,000 cells for the whole domain mesh after the final refinement has been implemented. To get a better comparison, the numerical results also are post processed with ParaFoam software [21] and the liquid interface meshes are rendered by Blender open-source software [22].

Results and Discussion

The trajectory of biodiesel and diesel are illustrated in Figure 4. In addition, the experimental shadowgraphs of the same operating condition [1] are depicted in the same figure for comparison. As can be seen, biodiesel jet has more bag shaped ligaments at the windward side of the jet. This fact is clear in the simulation results as well. Furthermore the biodiesel jet column in comparison to the diesel jet, in either the experimental and numerical results, has bent more before the column breakup. This behaviour is thought to be a result of experiencing higher drag on the biodiesel jet. Figure 5 shows velocity contours at different sections of the computational domain. As can be observed in this figure, there are stronger and wider wakes surrounding the biodiesel jet comparing to the diesel jet. Therefore the drag force causing by these wakes, can be translated into bending of the column jet of biodiesel. It should be mentioned that B50, which is not shown in Figure 4 has an intermediate behaviour between B100 and diesel in terms of jet bending and bag shape ligaments.

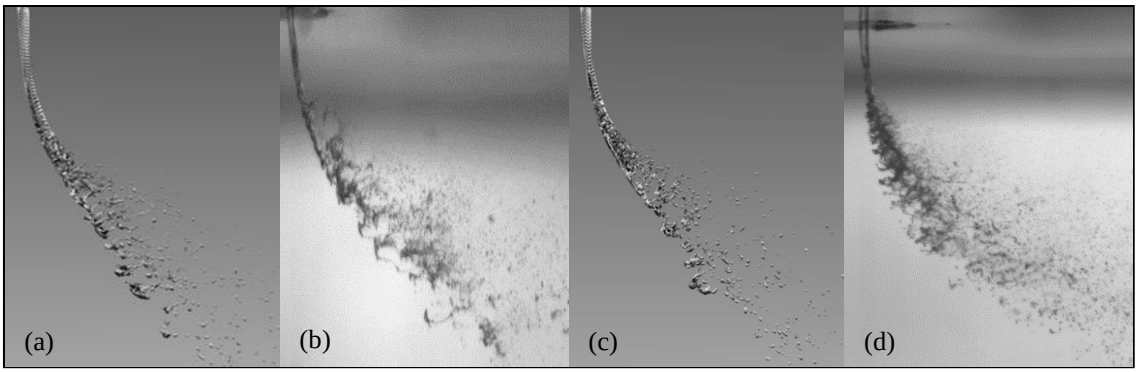

Figure 4 Numerical and experimental trajectories at We = 48, q = 100. B100 (a), numerical, (b) shadowgraph [1], diesel (c), numerical, (d), shadowgraph [1].

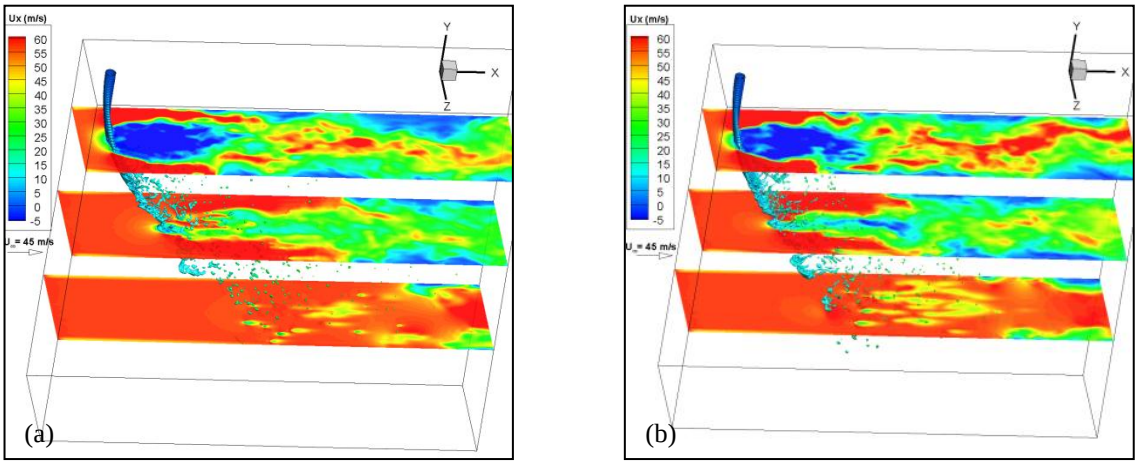

Figure 5 Velocity contours at We = 48, q = 100. (a) B100, (b) diesel.

Another interesting result is having more bag shape ligaments in the biodiesel spray comparing to the diesel spray as a result of primary breakup. This fact is clearly illustrated in Figure 6 that shows the liquid interface near the windward trajectory and just after the primary breakup. Having these bag shape ligaments at Weber

numbers even higher than 40 (We = 48), which is commonly known as the atomization regime, depicts how the high viscosity of biodiesel and its blends affects the primary breakup regime of biodiesel.

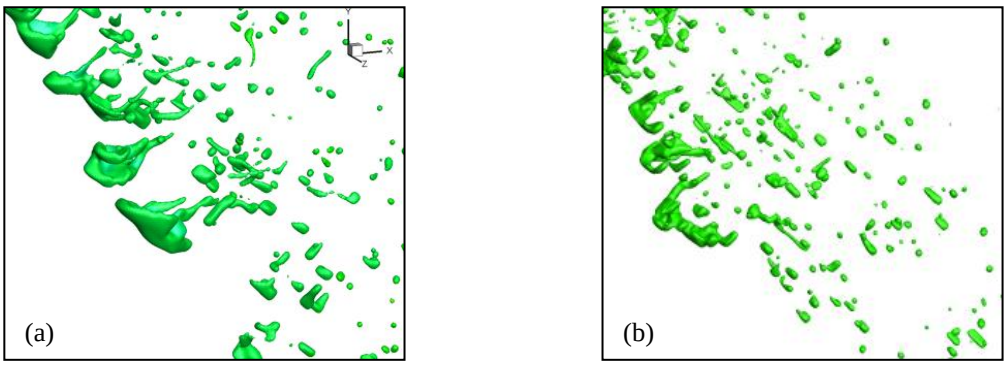

Figure 6 Snapshots of (a) biodiesel and (b) diesel just after the primary breakup

Figure 7 demonstrates the maximum velocity of droplets downstream of the computational domain, i.e. 40d or 20mm downstream of the injection point. Apparently, at the same operating condition, the diesel droplets have higher maximum and the B50 and B100 have lower maximum velocities respectively. These results once again confirm having stronger and wider wakes surrounding the biodiesel jet that consequently affects its droplets having lower velocities.

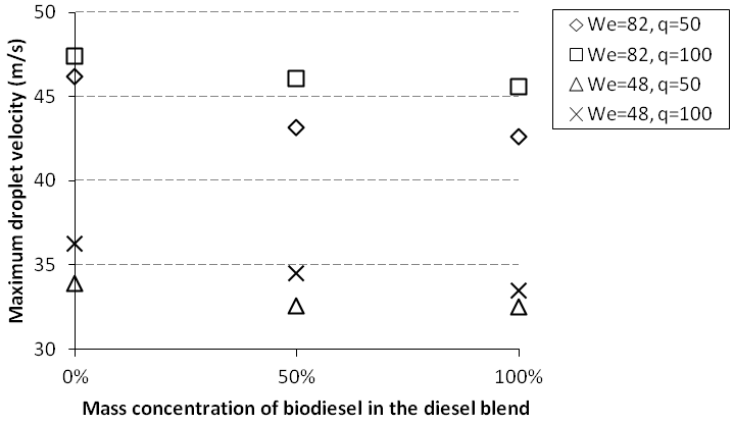

Figure 7 Maximum velocity of downstream droplets for diesel, B50 and B100 at different operating conditions.

The windward trajectories of different liquids are shown in Figure 8. As can be seen, the results of the numerical simulation are in good agreement (<±10% difference) with the experimental results [1]. Also it is clear that the maximum error of numerical results appear typically, downstream of the domain. This can be due to the oscillatory behaviour of the windward trajectory in different time steps at downstream locations where mostly, contains small droplets. It should be mentioned that the numerical trajectories of Figure 8 are the windward trajectories of the last numerical time step, while the experimental results of Figure 8 are an average of windward trajectories in 500 shadowgraph snapshots [1]. As another remarkable result in Figure 8, both the experimental and numerical results depict a decrease in the penetration depth from diesel to B50 and B100. This behaviour of the penetration depth for diesel, B50 and B100 can be translated in change of the spray mixing locus in the engine applications.

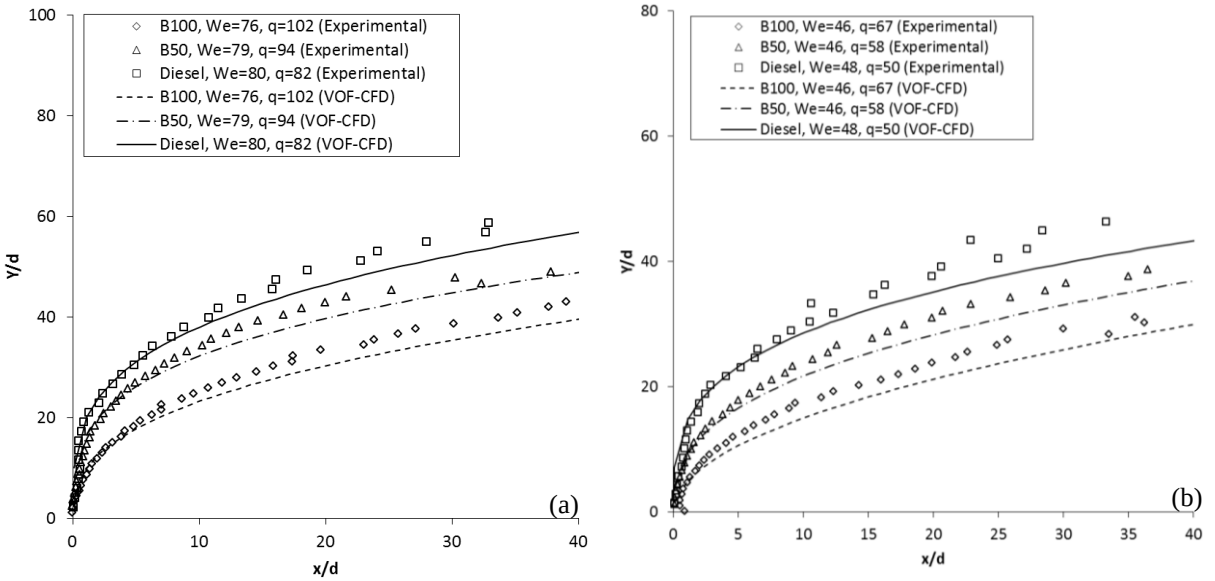

Figure 8, Numerical and experimental trajectories of diesel, biodiesel and their blend at different Weber numbers and momentum ratios

Figure 9 shows the comparison of different numerical methods with the experimental results [1]. Farvardin *et al.* [1] also performed a Lagrangian numerical simulation with the Discrete Phase Model (DPM) method. In the DPM method, the liquid part is not solved as a bulk fluid by the Navier Stokes equation. Instead the liquid part is modeled as a series of discrete droplets with a specified size at the injector exit. Subsequently, a set of empirical relations governs the discrete droplets in terms of secondary breakup, deformation, evaporation, etc. For example, in the above mentioned paper, they used Taylor Analysis Breakup (TAB) method to simulate the breakup of initial spherical droplets as in a spring-mass system. As a result and as mentioned in [1], this type of simulation, does not predict the penetration depth very well due to column jet bending, surface waves and primary breakup effect which are not modeled in DPM. In this study, the progress of the simulation results from DPM to VOF is shown in Figure 9. The VOF simulation results are significantly closer to the experimental results (±10% accurate) in comparison to the DPM results [1] (±35%).

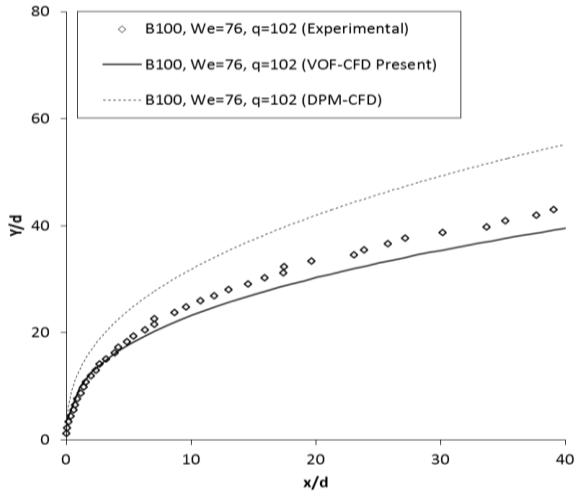

Figure 9 Comparison of different numerical simulations (VOF as present work and DPM as the previous work of the authors [1]) with the experimental results

Summary and Conclusions

A comparative study of B100, B50 and diesel jet in crossflow is performed by a coupled VOF-LES simulation. In addition the numerical results are validated by the same condition experimental results of the authors [1]. The results show lower penetration depth of biodiesel jet comparing to the diesel jet. This behaviour is assumed to be due to the larger drag acting on biodiesel liquid columns which bends the jet more towards the downstream. This is in a manner that diesel jet owing to smaller drag penetrates more inside the crossflow of air before complete bending towards the cross flowing air. Several bag shapes are observed after the primary breakup

of biodiesel at large Weber numbers, i.e. atomization Weber numbers, which argues the common classification of primary breakup regimes. This is in a manner that at the same Weber numbers, diesel show atomization mode of breakup. On the other hand, biodiesel droplets at downstream of the domain have lower velocities which can be as a result of having wider wakes surrounding the biodiesel column. Ultimately, the windward trajectory of VOF-LES simulation is compared with the DPM simulation results [1]. Apparently, the results of VOF-LES seem to be in better agreement with the experimental shadowgraph results in comparison with the DPM trajectories.

References

[1] E. Farvardin, M. Johnson, P. Gauthier, A. Dolatabadi, *Combustion Institute Canadian Section Conference*, Winnipeg, MB, 2011.
[2] A.K. Agarwal, *Progress in Energy and Combustion Science* 33: 233–271, (2007).
[3] J.P. Szybista, J. Songa, M. Alama, A.L. Boehman, *Fuel Processing Technology* 88:679-691, (2007).
[4] J.A. Schetz, A. Padhye, *AIAA Journal* 15: 1385-1390, (1977).
[5] P.K. Wu, K.A. Kirkendall, R.P. Fuller, A.S. Nejad, *Journal of Propulsion and Power* 14: 173-182, (1998).
[6] P.K. Wu, L.K. Tseng, G.M. Faeth, *Atomization and Sprays* 2: 295-317, (1992).
[7] P.K. Wu, K.A. Kirkendall, R.P. Fuller, A.S. Nejad, *Journal of Propulsion and Power* 13: 64-73, (1997).
[8] C.O. Iyogun, M. Birouk, N. Popplewell, *Atomization and Sprays* 16: 963-979, (2006).
[9] O.M. Elshamy, *Experimental Investigations of Steady and Dynamic Behaviour of Transverse Liquid Jets*, University of Cincinnati, Cincinnati, OH, USA, 2006.
[10] J. Stenzler, J.G. Lee, D. Santavicca, W. Lee, *Atomization and Sprays* 16: 887-906, (2006).
[11] Madabhushi, R.K., *Atomization and Sprays* 13: 413-424, (2003).
[12] Aalburg, C., Metwally, H.M., Ng, C-L, Sallam, K.A., *AIAA Journal* 42-12: 2529-2540, (2005).
[13] Herrmann, M., *ASME Journal of Engineering for Gas Turbine and Power* 132-6: 061506.1-10, (2010).
[14] Schumacher, L., *The Physical and Chemical Characterization of Biodiesel Low Sulfur Blends*, Report for National Biodiesel Board, University of Missouri, 1995.
[15] A. Ahmed, C.E. Ejim, B.A. Fleck, A. Amirfazli, *SAE 2006 World Congress*, SAE Tech. Paper 2006-01-0893, Detroit, MI, USA, April 2006.
[16] R, Scardovelli, S. Zaleski, *Annual Review of Fluid Mechanics*, 31: 567-603, (1999).
[17] A., Yoshizawa, K., Horiuti, *Journal of the Physical Society of Japan* 54: 2834-2839, 1985.
[18] H., Rusche, *Computational Fluid Dynamics of Dispersed Two Phase Flows at High Phase Fractions*, PhD Thesis, Imperial College University of London, 2002.
[19] N., Spyrou, D., Choi, A., Sadiki, J., Janicka, *Seventh International Conference on Multiphase Flow (ICMF)*, Florida, May 2010.
[20] www.openfoam.com
[21] www.paraview.org
[22] www.blender.org